Video Article

Microfluidic Platform with Multiplexed Electronic Detection for Spatial Tracking of Particles

Ningquan Wang[1], Ruxiu Liu[1], A. Fatih Sarioglu[1,2,3]

[1]School of Electrical and Computer Engineering, Georgia Institute of Technology

[2]Institute of Electronics and Nanotechnology, Georgia Institute of Technology

[3]Petit Institute for Bioengineering and Biosciences, Georgia Institute of Technology

Correspondence to: A. Fatih Sarioglu at sarioglu@gatech.edu

URL: https://www.jove.com/video/55311
DOI: doi:10.3791/55311

Keywords: Bioengineering, Issue 121, lab-on-a-chip, microfluidics, multiplexed cytometry, spatial cell tracking, resistive pulse sensing, Coulter counter, CDMA, orthogonal detection

Date Published: 3/13/2017

Citation: Wang, N., Liu, R., Sarioglu, A.F. Microfluidic Platform with Multiplexed Electronic Detection for Spatial Tracking of Particles. *J. Vis. Exp.* (121), e55311, doi:10.3791/55311 (2017).

Abstract

Microfluidic processing of biological samples typically involves differential manipulations of suspended particles under various force fields in order to spatially fractionate the sample based on a biological property of interest. For the resultant spatial distribution to be used as the assay readout, microfluidic devices are often subjected to microscopic analysis requiring complex instrumentation with higher cost and reduced portability. To address this limitation, we have developed an integrated electronic sensing technology for multiplexed detection of particles at different locations on a microfluidic chip. Our technology, called Microfluidic CODES, combines Resistive Pulse Sensing with Code Division Multiple Access to compress 2D spatial information into a 1D electrical signal. In this paper, we present a practical demonstration of the Microfluidic CODES technology to detect and size cultured cancer cells distributed over multiple microfluidic channels. As validated by the high-speed microscopy, our technology can accurately analyze dense cell populations all electronically without the need for an external instrument. As such, the Microfluidic CODES can potentially enable low-cost integrated lab-on-a-chip devices that are well suited for the point-of-care testing of biological samples.

Video Link

The video component of this article can be found at https://www.jove.com/video/55311/

Introduction

Accurate detection and analysis of biological particles such as cells, bacteria or viruses suspended in liquid is of great interest for a range of applications[1,2,3]. Well-matched in size, microfluidic devices offer unique advantages for this purpose such as high-sensitivity, gentle sample manipulation and well-controlled microenvironment[4,5,6,7]. In addition, microfluidic devices can be designed to employ a combination of fluid dynamics and force fields to passively fractionate a heterogeneous population of biological particles based on various properties[8,9,10,11,12]. In those devices, the resultant particle distribution can be used as readout but spatial information is typically accessible only through microscopy, limiting the practical utility of the microfluidic device by tying it to a lab infrastructure. Therefore, an integrated sensor that can readily report particles' spatiotemporal mapping, as they are manipulated on a microfluidic device, can potentially enable low-cost, integrated lab-on-a-chip devices that are particularly attractive for the testing of samples in mobile, resource-limited settings.

Thin film electrodes have been used as integrated sensors in microfluidic devices for various applications[13,14]. Resistive Pulse Sensing (RPS) is particularly attractive for integrated sensing of small particles in microfluidic channels as it offers a robust, sensitive, and high-throughput detection mechanism directly from electrical measurements[15]. In RPS, the impedance modulation between a pair of electrodes, immersed in an electrolyte, is used as a means to detect a particle. When the particle passes through an aperture, sized on the order of the particle, the number and amplitude of transient pulses in the electrical current are used to count and size particles, respectively. Moreover, the sensor geometry can be designed with a photolithographic resolution to shape resistive pulse waveforms in order to enhance sensitivity[16,17,18,19] or to estimate vertical position of particles in microfluidic channels[20].

We have recently introduced a scalable and simple multiplexed resistive pulse sensing technology called Microfluidic Coded Orthogonal Detection by Electrical Sensing (Microfluidic CODES)[21]. Microfluidic CODES relies on an interconnected network of resistive pulse sensors, each consisting of an array of electrodes micromachined to modulate conduction in a unique, distinguishable manner, so as to enable multiplexing. We have specifically designed each sensor to produce orthogonal electrical signals similar to the digital codes used in code division multiple access[22] (CDMA) telecommunication networks, so that individual resistive pulse sensor signal can be uniquely recovered from a single output waveform, even if signals from different sensors interfere. In this way, our technology compresses 2D spatial information of particles into a 1D electrical signal, permitting monitoring of particles at different locations on a microfluidic chip, while keeping both device- and system-level complexity to a minimum.

In this paper, we present a detailed protocol for experimental and computational methods necessary to use the Microfluidic CODES technology, as well as representative results from its use in analysis of simulated biological samples. Using the results from a prototype device with four multiplexed sensors as an example to explain the technique, we provide protocols on (1) the microfabrication process to create microfluidic devices with the Microfluidic CODES technology, (2) the description of the experimental setup including the electronic, optical, and fluidic hardware, (3) the computer algorithm for decoding interfering signals from different sensors, and (4) the results from detection and analysis of cancer cells in microfluidic channels. We believe that using the detailed protocol described here, other researchers can apply our technology for their research.

Protocol

1. Design of Coding Electrodes

Note: Figure 1a shows the 3-D structure of the micropatterned electrodes.

1. Design a set of four 7-bit Gold codes for encoding the microfluidic channels[23].
    1. Construct two linear feedback shift-registers (LFSRs), each representing a primitive polynomial.
    2. Use the LFSRs to generate a preferred pair of 7-bit *m*-sequences.
    3. Cyclically shift the preferred pair of *m*-sequences and add them in mod 2 to generate four distinct Gold codes.

2. Design the layout of the coding electrodes (**Figure 1b**).
    1. Place three electrode terminals, representing the positive, negative, and reference electrodes at three corners.
    2. Route positive and negative electrode traces on opposite sides of each microfluidic channel.
    3. Extend positive and negative electrodes into the microfluidic channels as electrode fingers, following the uniquely assigned Gold code (**Figure 1c**).
    4. Place the reference electrode in between the positive and negative electrode fingers.
    5. Place positive and negative electrode traces far from the outermost reference electrode fingers in order to minimize electrical conduction outside the coding region.

2. Microfabrication of Surface Electrodes

Note: Figure 2b shows the fabrication process of surface electrodes.

1. Clean a 4-inch borosilicate glass wafer in a piranha solution (98% sulfuric acid : 30% hydrogen peroxide = 5 : 1) at 120 °C for 20 min to remove all the organic contaminants. Then place the wafer on a 200 °C hot plate for 20 min to remove residual water.
2. Transfer the wafer to a spinner. Dispense 2 mL negative photoresist onto the wafer and spin the wafer at a speed of 3,000 rpm for 40 s to uniformly coat the wafer with a 1.5-µm photoresist layer.
3. Place the wafer on a 150 °C hot plate and bake the spun photoresist for 1 min.
4. Expose the photoresist to 365-nm UV light (225 mJ/cm^2) through a chrome mask using a mask aligner.
5. Place the wafer on a 100 °C hot plate and bake the exposed photoresist for 1 min.
6. Develop the photoresist by immersing the wafer in a photoresist developer (RD6) for 15 s. Gently spray deionized (DI) water and wash the wafer. Dry by blowing compressed nitrogen.
7. Place the wafer with patterned photoresist into an e-beam metal evaporator, and deposit a 20-nm-thick chrome film, followed by an 80-nm-thick gold film onto the wafer at a base pressure of 3×10^{-6} Torr with a deposition rate of 1 Å/s.
8. Immerse the metal-coated wafer into acetone in an ultrasonic bath set at a frequency of 40 kHz with 100% amplitude for 30 min at room temperature to etch the underlying photoresist and complete the lift-off process.
9. Dice the wafer into smaller pieces using a conventional dicing saw.

3. Fabrication of the SU-8 Mold for Microfluidic Channels

Note: Figure 2a shows the fabrication process of the mold for microfluidic channels.

1. Clean and bake a 4-inch silicon wafer using the same procedure described in 2.1.
2. Transfer the wafer to a spinner. Pour 4 mL photoresist onto the wafer. Coat the wafer with photoresist.
    1. Spin the wafer at 500 rpm for 15 s.
    2. Spin the wafer at 1,000 rpm for 15 s.
    3. Spin the wafer at 3,000 rpm for 60 s to obtain a uniformly coated 15-µm thick photoresist layer.

3. Place the wafer face up on a cleanroom wipe soaked in acetone and remove the residual photoresist from the backside and edges of the wafer.
4. Transfer the wafer onto a hot plate for soft baking. First, bake the wafer at 65 °C for 1 min. Then quickly move the wafer to a 95 °C hot plate and bake for 2 min.
5. Expose the photoresist to 365-nm UV light (180 mJ/cm^2) through a chrome mask by using a mask aligner.
6. Bake the wafer following exposure at 65 °C for 1 min and then at 95 °C for 2 min.
7. Immerse the wafer in developer and gently shake the container for 3 min. Then, rinse the wafer with isopropanol alcohol (IPA) and dry it by blowing compressed nitrogen. If a white-colored residue appears on the wafer, immerse it into the developer again and develop for longer time and dry.
8. Bake the wafer on a 200 °C hot plate for 30 min to dry it completely.

9. Measure the thickness of the patterned photoresist using a profilometer at different locations across the wafer to ensure uniformity.
10. Silanize the mold wafer by utilizing the technique of vapor deposition. Add 200 µL of trichlorosilane in a Petri dish and place in a vacuum desiccator along with the SU-8 mold wafer for 8 h.

4. Assembly of the Microfluidic CODES Device

1. Place the 4-inch silicon wafer with the mold in a 150-mm diameter Petri dish, and fix it by taping from its edges.
2. Mix the polydimethylsiloxane (PDMS) pre-polymer and cross-linker at a ratio of 10:1, and pour 50 g of the mixture into the Petri dish. Place the Petri dish in a vacuum desiccator to degas the mixture for 1 h, and then cure it in an oven at 65 °C for at least 4 h (**Figure 2a**).
3. Cut out the cured PDMS layer using a scalpel and peel it off the mold wafer using a tweezer. The size of the proof-of-principle device is approximately 20 mm × 7 mm. Then punch holes with a diameter of 1.5 mm through the PDMS for the inlet and outlet of the microfluidic channel using a biopsy puncher.
4. Clean the patterned side of the PDMS part by placing it on a clean-room adhesive tape.
5. Clean the glass substrate with surface electrodes by rinsing it with acetone, IPA, DI water and dry using compressed nitrogen.
6. Activate the surfaces of PDMS and glass substrate in oxygen plasma for 30 s with the micromachined side of each part facing up in an RF plasma generator set at 100 mW.
7. Align the PDMS microfluidic channel with surface electrodes on the glass substrate using an optical microscope and then bring the two plasma-activated surfaces in physical contact.
8. Bake the device on a 70 °C hot plate for 5 min, with the glass side facing the hot plate.
9. Connect the contact pads of the electrodes with wires by soldering.

5. Preparation of the Simulated Biological Sample

1. Culture the HeyA8 human ovarian cancer cells in RPMI 1640 supplemented with 10% fetal bovine serum (FBS) and 1% penicillin-streptomycin in 5% CO_2 atmosphere at 37 °C until they reach 80% confluence.
2. Aspirate the media from the culture flask using a glass pipette. Dispense and then aspirate 1x phosphate buffered saline (PBS) to wash the cells.
3. Incubate cells in 2 mL 0.05% (w/v) trypsin solution for 2 min at 37 °C to suspend adherent cells. Then, add 4 mL of the culture media to neutralize the trypsin.
4. Centrifuge the cell suspension at 100 × g for 5 min to pellet the cells in a test tube. Then, aspirate supernatant completely.
5. Re-suspend the cells in 1-2 mL 1x PBS by gently pipetting up and down to mechanically dissociate cell clumps.
6. Draw a small amount of cell suspension into a pipette and count the number of cells using hemocytometer.
7. Dilute the cell suspension with PBS to prepare a sample with final cell concentration of 10^5-10^6 cells/mL.

6. Running the Microfluidic CODES Device

Note: Figure 3 shows the experimental setup.

1. Place the Microfluidic CODES device on the stage of an optical microscope.
2. Apply a 400 kHz sine wave to the reference electrode on the chip using an electronic function generator.
3. Connect positive and negative sensing electrodes to two independent trans-impedance amplifiers to convert current signals from each to voltage signals.
4. Subtract the positive sensing electrode voltage signal from the negative sensing electrode voltage signal using a differential voltage amplifier in order to obtain a bipolar signal.
5. Use a high-speed camera to optically record operation of the device for validation and characterization purposes.
6. Drive the cell suspension through the Microfluidic CODES device at a constant flow rate (50-1,000 µL/h) using a syringe pump.
7. Measure the impedance modulation signal using a lock-in amplifier.
    1. Connect the reference AC signal to the reference input of the lock-in amplifier. Connect the differential bipolar signal to the lock-in amplifier as input signal.
    2. Obtain the RMS amplitude of the differential signal from the lock-in amplifier output.
8. Sample the lock-in amplifier output signal at 1 MHz rate into a computer through a data acquisition board for further analysis.

7. Processing of Sensor Signals

1. Transfer recorded electrical data into MATLAB for post-processing and decoding.
2. Filter the recorded signal in the digital domain using a Butterworth filter (MATLAB built-in function) to remove the high frequency noise (>2.5 kHz).
3. Generate a template code library from sensor signals.
    1. Identify representative non-overlapping code signals corresponding to each sensor in the device and extract these signal blocks from the dataset as separate waveform vectors.
    2. Normalize each template code waveform vector by its power. Use the MATLAB built-in function (bandpower) to measure the signal power.
    3. Use MATLAB function (resample) to expand the template library by digitally creating versions of normalized code signals with varying durations to accommodate variations in the cell flow speed over the electrodes.
4. Identify the signal blocks that correspond to sensor activity (threshold: SNR > 12 dB) in the filtered waveform. Waveform with SNR under the threshold would be treated as noise.

5. Decode individual blocks of sensor activity in the recorded signal by using an iterative algorithm based on the successive interference cancellation, a technique commonly employed in multi-user CDMA communication networks[24,25].
    1. Calculate cross-correlation of each signal block with all of the templates in the library using sliding dot product.
    2. Identify the template that produces the largest auto-correlation peak to determine the dominant individual sensor code signal. Record the both time and amplitude of the autocorrelation peak.
    3. Construct an estimate sensor code signal by scaling the identified code template based on the measured autocorrelation peak amplitude and timing information (determined in step 7.5.2).
    4. Subtract the estimated sensor code signal from the original data.
    5. Iterate the process from 7.5.1, until the residual signal does not resemble any signal in the template library, mathematically defined as the correlation coefficient being less than 0.5.

6. Refine initial sensor signal estimations from step 7.5 using an optimization process.
    1. Reconstruct the signal by adding estimated individual sensor signals from each iteration.
    2. Sweep the amplitude, duration and timing of individual sensor signals around the original estimates to produce the best fit with the recorded electrical signal based on least-squares approximation[26].

7. Convert amplitudes of estimated sensor signals into cell size by calibrating electrical signals against optical images.

Representative Results

A Microfluidic CODES device consisting of four sensors distributed over four microfluidic channels is shown in **Figure 1b**. In this system, the cross-section of each microfluidic channel was designed to be close to the size of a cell so that (1) multiple cells cannot pass over the electrodes in parallel and (2) cells remain close to the electrodes increasing the sensitivity. Each sensor is designed to generate a unique 7-bit digital code. The device was then tested using a cell suspension. Recorded electrical signals corresponding to four individual sensors are shown with associated ideal digital codes in **Figure 4**. Recorded signals closely match with the ideal square pulses, while small deviations do exist. Such deviations result from a combination of several factors including the non-uniform electric field between coplanar electrodes, coupling between different electrode pairs, spherical shape of cells, as well as the constant flow speed of cells in microfluidic channels. We created a template library based on the recoded sensor signals. By correlating the recorded signals with all of the templates in the library, we determined a template that produced the maximum auto-correlation peak (**Figure 4**). As the digital codes for microfluidic channels are designed to be orthogonal to each other, a dominant auto-correlation peak could robustly be identified in this process. Using this approach, we could computationally determine the microfluidic channel the cell passed through, the duration of the sensor signal, and therefore the flow speed of the cell.

The Microfluidic CODES technology can resolve situations when multiple cells simultaneously interact with coding electrodes. When such overlaps occur, the signals from individual sensors interfere and the resultant waveform cannot readily be associated with any single template corresponding to a specific sensor. Accurately decoding such overlapping signals is particularly important for reliable processing high-density samples, where interferences are more likely to occur. To resolve overlapping events, we developed an iterative algorithm based on a successive interference cancellation (SIC) scheme[24,25], which is typically used for multi-user detection in CDMA communication networks. **Figure 5** demonstrates how the SIC algorithm is implemented in resolving a waveform that resulted from four overlapping cells in four different microfluidic channels. In each iteration, we first determined the dominant auto-correlation peak (**Figure 5a**, 2nd column), corresponding to the strongest interfering signal, by correlating the input waveform (**Figure 5a**, 1st column) with the template library. Based on the selected template and the resultant auto-correlation amplitude, we then estimated the strongest interfering signal (**Figure 5a**, 3rd column) and subtracted it from the input waveform. The remaining waveform was passed to the next iteration as the input. This process continued until the correlation of the residual signal with the template library did not produce a clear auto-correlation peak (**Figure 5a**, 5th row, 2nd plot). Following the termination of the interference cancellation process, we reconstructed an estimate of the waveform by combining all the estimated signals from each iteration (**Figure 6a**). Using an optimization process based on a least squares approximation to minimize the mean square error between the original waveform and the reconstructed signal, we updated our estimates for the amplitude, duration, and relative timing of individual sensor code signals (**Figure 6b**). We also estimated the size of the cells detected based on the amplitude of the estimated individual sensor signals. To achieve this, we calibrated the electrical signal amplitudes with optically measured cell sizes using linear regression (**Figure 6b**). A comparison of our results from the Microfluidic CODES with the information obtained from the simultaneously recorded high-speed microscope images shows that the cell size and speed can be accurately measured, which validates our results (**Table 1**). **Figure 6c** shows the simultaneously recorded high-speed microscopy image used for validating the decoding result.

To demonstrate the reproducibility of our results and also the performance of the Microfluidic CODES technology for a high-throughput sample processing, we analyzed electrical signals corresponding to >1,000 cells. The signals were automatically decoded in MATLAB by running the algorithm explained above and the accuracy of our results was evaluated by directly comparing our results with optical data from simultaneously recorded high-speed video. Our analysis indicates that electrical signals from 96.15% of cells (973/1,012) were accurately decoded. Success rate for decoding non-overlapping and overlapping cell signals is 98.71% (688/697) and 90.48% (285/315), respectively.

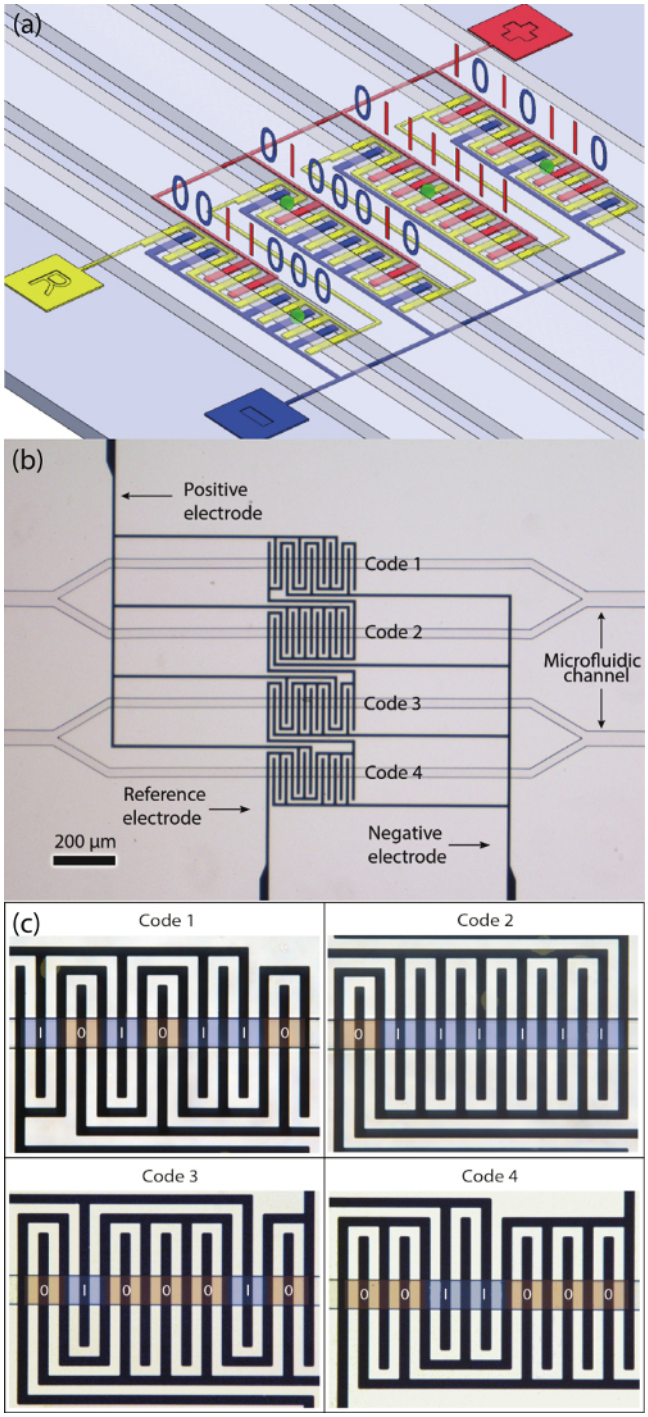

Figure 1. Design of the four-channel Microfluidic CODES device. (**a**) Electrodes in each microfluidic channel are micropatterned to generate a unique digital code. The impedance modulation due to sequential interactions of flowing cells with electrode pairs leads to electrical pulses. (**b**) A microscope image of the Microfluidic CODES device. During the fabrication process, glass substrate with coding surface electrodes is aligned with PDMS microfluidic channels under a microscope. (**c**) A close-up image of coded surface electrodes producing 7-bit Gold sequences: "1010110", "0111111", "0100010", "0011000". Please click here to view a larger version of this figure.

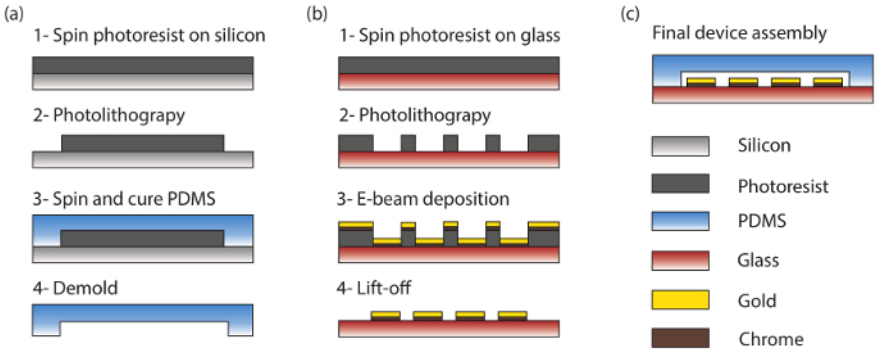

Figure 2. Microfabrication process. (**a**) The PDMS microfluidic channels are fabricated using soft lithography[27]. (**b**) The surface electrodes are fabricated using a lift-off process. (**c**) A cross-sectional schematic of the final device. PDMS microfluidic channels are aligned and bonded to the glass substrate with surface electrodes. Please click here to view a larger version of this figure.

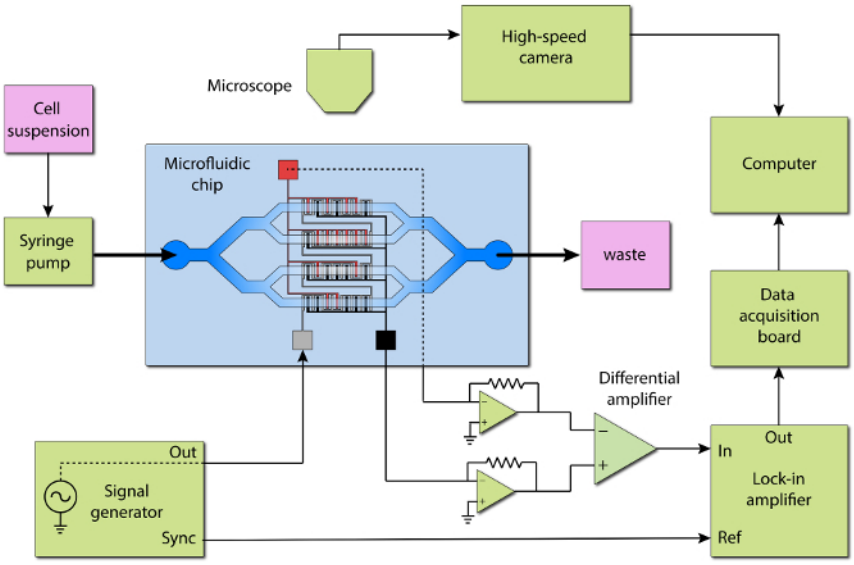

Figure 3. Experimental setup. Using a syringe pump, the cell suspension is run through the Microfluidic CODES device at a constant flow rate. A 400 kHz AC signal is applied to the reference electrode using a function generator. Current signals from positive and negative sensing electrodes are first converted into voltage signals using two transimpedance amplifiers and subtracted from each other using a differential amplifier. The differential bipolar signal is extracted by a lock-in amplifier and then sampled into a computer for signal processing and decoding. High-speed optical microscopy is used to optically record operation of the device for validation and characterization purposes. Please click here to view a larger version of this figure.

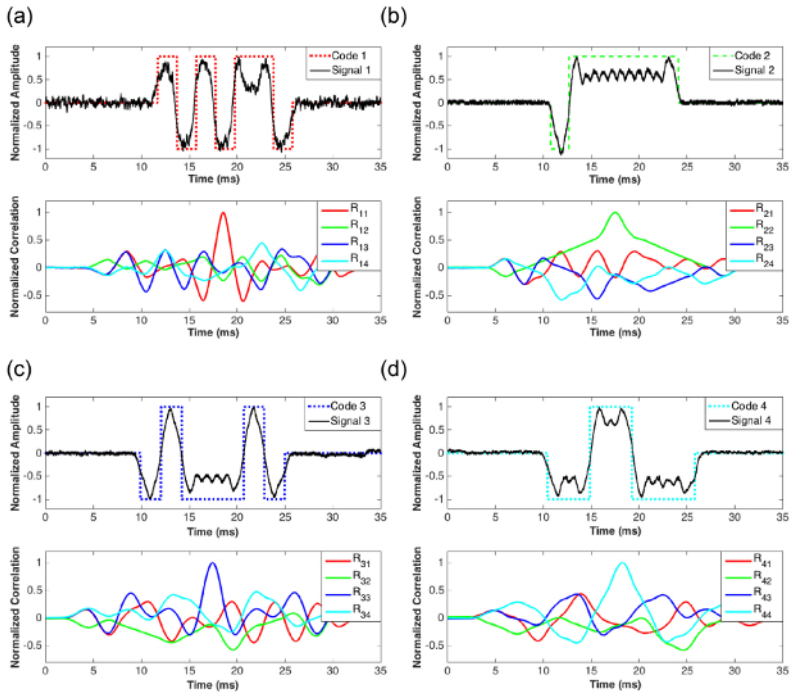

Figure 4. Recorded electrical signals from individual sensors and their correlations. Recorded signals and their correlation with each other are given for four code-multiplexed resistive pulse sensors. Sensor 1 (**a**), sensor 2 (**b**), sensor 3 (**c**) and sensor 4 (**d**) were designed to produce 7-bit digital waveforms "1010110", "0111111", "0100010", and "0011000", respectively. For each sensor, the top figure shows that normalized signal recorded from each sensor matches closely with the ideal square pulse sequence that the sensor was designed to produce. For each sensor, the lower panel shows recorded sensor signal's autocorrelation and cross-correlation with signals corresponding to three other code-multiplexed sensors in the network. In all cases, an autocorrelation peak can robustly be identified because the digital codes from individual sensors are designed to be orthogonal to each other. Please click here to view a larger version of this figure.

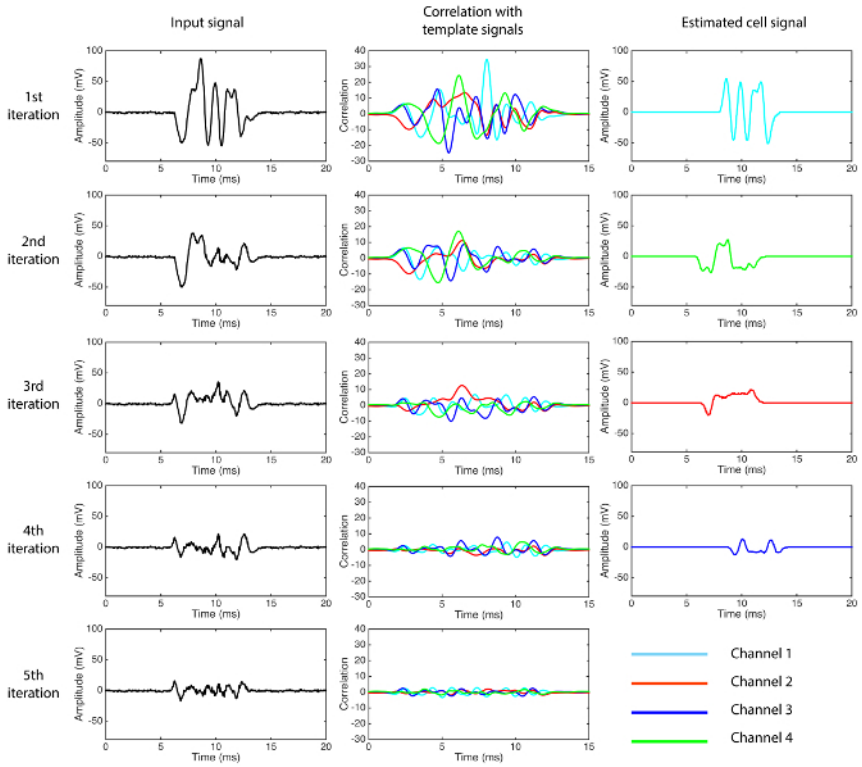

Figure 5. Decoding an overlapping waveform with successive interference cancelation. In each iteration, the input waveform (1st column) is correlated with the preassembled template library to identify the specific template that results in the maximum correlation amplitude (2nd column). Using this specific template, the strongest interfering signal is estimated based on the amplitude and timing information from the correlation peak (3rd column). The estimated signal is then subtracted from the original waveform, effectively canceling the strongest interference due to the largest cell. The process is iterated until no correlation peak can be determined (*i.e.*, correlation coefficient < 0.5) in the residual signal. Please click here to view a larger version of this figure.

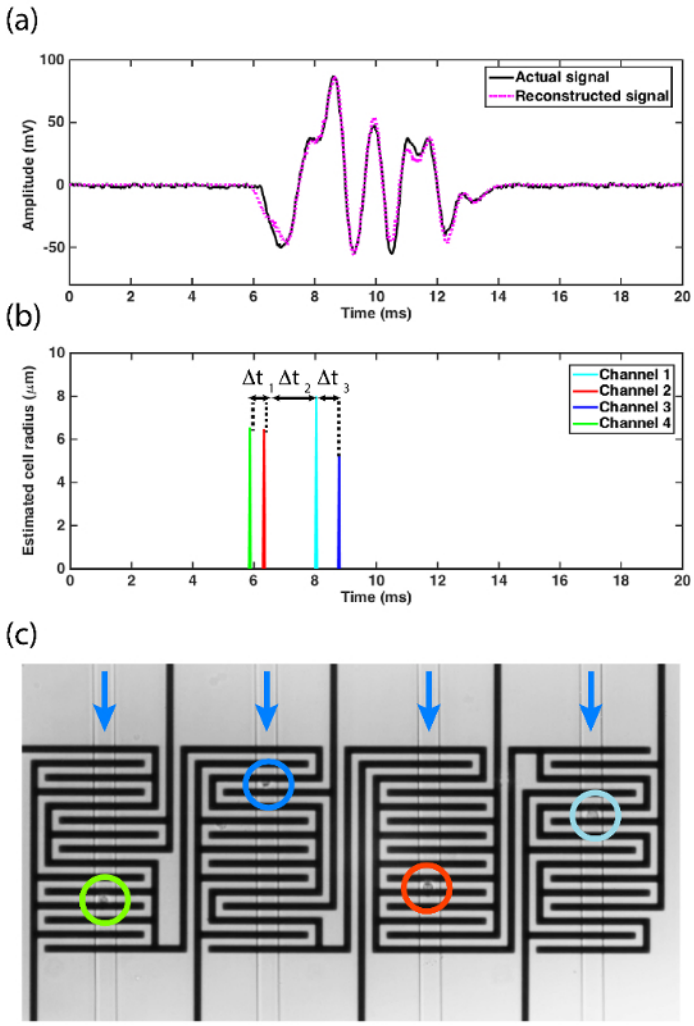

Figure 6. Decoding result analysis. (**a**) Estimated signals are refined based on an optimization algorithm that aims to obtain the best fit between the reconstructed and the original recorded waveform using the least-squares approximation. (**b**) At the end of the optimization process, the timing and amplitude of calibrated signals accurately reflect the cell parameters measured by high-speed microscopy. (**c**) Simultaneously recorded high-speed microscopy image validates our results from electrical measurements. Please click here to view a larger version of this figure.

Measurement type	r_{ch1} (μm)	r_{ch2} (μm)	r_{ch3} (μm)	r_{ch4} (μm)	Δt_1 (ms)	Δt_2 (ms)	Δt_3 (ms)
Electrical	8.010	6.490	5.300	6.550	0.465	1.705	0.744
Optical	8.320	6.770	5.680	7.040	0.375	1.625	0.750

Table 1. Comparison of electrically and optically measured cell parameters of Figure 6b. To validate our estimations, we optically measured the cell sizes from the high-speed microscopy image. Relative timing between different cells is optically measured from the number of frames between the cells in the high-speed video recorded at 8,000 frames per second.

Discussion

Multiple resistive pulse sensors have previously been incorporated into microfluidic chips[28,29,30,31,32]. In these systems, resistive pulse sensors were either not multiplexed[28,29,30,31] or they required individual sensors to be driven at different frequencies[32]. In both cases, dedicated external connections were needed for each resistive pulse sensor on the chip and therefore a large number of sensors could not be integrated without greater hardware complexity. The important advantage of Microfluidic CODES is that it allows simultaneous reading of multiple resistive pulse sensors from a single output in a simple device. We achieve this by utilizing multiplexing techniques commonly used in telecommunications to design micromachined resistive pulse sensors integrated into microfluidic devices. In essence, our technology relies on code-multiplexing a network of on-chip Coulter counters by designing each to produce a distinguishable signal when a particle is detected. Each micromachined sensor in the network consists of multiple coplanar surface electrodes ordered in differing configurations such that the sequential interaction of flowing particles with these electrodes produces orthogonal impedance modulations waveforms. To accommodate asynchronous particle-sensor interaction, we specifically designed each sensor to produce Gold codes[33], pseudo-orthogonal digital codes that are typically used in the uplink

of the CDMA telecommunication networks. Gold codes maintain a certain level orthogonality even when they are misaligned with random phase differences[34].

Microfluidic CODES is easily scalable. Although we presented results from a prototype Microfluidic CODES device with four sensors in this paper, more sensors can be incorporated in the device when designed to produce output signals distinguishable from the rest. One way to expand the sensor network is to design sensors based on larger orthogonal code sets with longer digital codes. Longer orthogonal codes with more bits provide higher processing gain in decoding and can be distinguished from each other when there is interference. On the other hand, longer Gold codes in the device also means larger sensing volume, which increases the expected number of interfering sensors. Likewise, increasing the number of sensors for a given sample density will lead to more particles overlapping due to an increase in the overall sensing volume. As such, the density of the particles in the sample is a critical parameter that needs to be considered in using the Microfluidic CODES technology. The maximum particle density that can be resolved (in analogy with the channel capacity of a CDMA telecommunications network) depends on several factors such as the individual sensor signals and their relation, the decoding scheme, layout of the microfluidic device, and the electronic noise level. Depending on the application, the sample can be diluted to reach a particle density that produces an acceptable error rate.

From signal processing perspective, decoding of time waveforms from a Microfluidic CODES device is not computationally intensive using current systems as evidenced by the fact that cell phone communications on a CDMA network can be demultiplexed in real-time. Furthermore, the physical events to be decoded in microfluidic devices happen much slower than bit transmission rate in cell phone communications allowing us to use more advanced and time-consuming algorithms such as SIC and an optimization processes, which we use to iteratively resolve overlapping signals from sensors.

Taken together, Microfluidic CODES is a versatile, scalable electronic sensing technology that can be readily integrated into various microfluidic devices to realize quantitative assays by tracking particles as they are processed on the chip. The technology is very easy to implement, because (1) it is very simple from a hardware perspective (2) it is directly compatible with the soft lithography (3) it provides a direct electronic read-out without any active on-chip component, and (4) it relies on simple computational algorithms for signal processing and data interpretation.

Disclosures

The authors have nothing to disclose.

Acknowledgements

This work was supported by National Science Foundation Award No. ECCS 1610995. The authors would like to thank the Institute of Electronics and Nanotechnology and the Parker H. Petit Institute for Bioengineering and Bioscience staff for their support in using shared facilities. The authors also would like to thank Chia-Heng Chu for his help in preparing the manuscript.

References

1. De Roy, K., Clement, L., Thas, O., Wang, Y., & Boon, N. Flow cytometry for fast microbial community fingerprinting. *Water Res.* **46** (3), 907-919 (2012).
2. Vives-Rego, J., Lebaron, P., & Nebe-von Caron, G. Current and future applications of flow cytometry in aquatic microbiology. *FEMS Microbiol Rev.* **24** (4), 429-448 (2000).
3. Alvarez-Barrientos, A., Arroyo, J., Cantón, R., Nombela, C., & Sánchez-Pérez, M. Applications of flow cytometry to clinical microbiology. *Clin Microbiol Rev.* **13** (2), 167-195 (2000).
4. Toner, M., & Irimia, D. Blood-on-a-chip. *Annu Rev Biomed Eng.* **7**, 77-103 (2005).
5. Mehling, M., & Tay, S. Microfluidic cell culture. *Current Opin Biotech.* **25**, 95-102 (2014).
6. Sarioglu, A. F., et al. A microfluidic device for label-free, physical capture of circulating tumor cell clusters. *Nat Methods.*, **12** (7), 685-691 (2015).
7. Cermak, N., et al. High-throughput measurement of single-cell growth rates using serial microfluidic mass sensor arrays. *Nat Biotechnol.* (2016).
8. Gossett, D. et al. Label-free cell separation and sorting in microfluidic systems. *Anal Bioanal Chem.* **397** (8), 3249-3267 (2010).
9. Tsutsui, H., & Ho, C. Cell separation by non-inertial force fields in microfluidic systems. *Mech Res Commun.* **36** (1), 92-103 (2009).
10. Edwards, T. L., Gale, B. K., & Frazier, A. B. A microfabricated thermal field-flow fractionation system. *Anal Chem.*, **74** (6), 1211-1216 (2002).
11. Wang, M. M. et al. Microfluidic sorting of mammalian cells by optical force switching. *Nat Biotechnol.*, **23** (1), 83-87 (2005).
12. Shields IV, C. W., Reyes, C. D., & López, G. P. Microfluidic cell sorting: a review of the advances in the separation of cells from debulking to rare cell isolation. *Lab Chip.* **15** (5), 1230-1249 (2015).
13. Gawad, S., Schild, L., & Renaud, P. Micromachined impedance spectroscopy flow cytometer for cell analysis and particle sizing. *Lab Chip.* **1** (1), 76-82 (2001).
14. Haandbæk, N., Bürgel, S. C., Heer, F., & Hierlemann, A. Characterization of subcellular morphology of single yeast cells using high frequency microfluidic impedance cytometer. *Lab Chip.* **14** (2), 369-377 (2014).
15. Bayley, H., & Martin, C. Resistive-pulse sensing-from microbes to molecules. *Chem Rev.* **100** (7), 2575-2594 (2000).
16. Polling, D., Deane, S. C., Burcher, M. R., Glasse, C., & Reccius, C. H. Coded electrodes for low signal-noise ratio single cell detection in flow-through impedance spectrophy. *Proceedings of uTAS.* (The 14th International Conference on Miniaturized Systems for Chemistry and Life Sciences), October 3-7, 2010, Groningen, The Netherlands. (2010).
17. Javanmard, M., & Davis, R. W. Coded corrugated microfluidic sidewalls for code division multiplexing. *IEEE Sensors J.* **13** (5), 1399-1400 (2013).

18. Balakrishnan, K. R. et al. Node-pore sensing: a robust, high-dynamic range method for detecting biological species. *Lab Chip.* **13** (7), 1302-1307 (2013).
19. Emaminejad, S., Talebi, S., Davis, R. W., & Javanmard, M. Multielectrode sensing for extraction of signal from noise in impedance cytometry. *IEEE Sensors J.* **15** (5), 2715-2716 (2015).
20. Spencer, D., Caselli, F., Bisegna, P., & Morgan, H. (2016). High accuracy particle analysis using sheathless microfluidic impedance cytometry. *Lab Chip.* **16**, 2467-2473 (2016).
21. Liu, R., Wang, N., Kamili, F., & Sarioglu, A. Microfluidic CODES: a scalable multiplexed electronic sensor for orthogonal detection of particles in microfluidic channels. *Lab Chip.* **16** (8), 1350-1357 (2016).
22. Buehrer, R. Code Division Multiple Access (CDMA). *Synthesis Lectures on Communications.* **1** (1), 1-192 (2006).
23. Proakis, J. *Digital Communications.*, McGraw-Hill, New York, NY (1989).
24. Patel, P., & Holtzman, J. Analysis of a simple successive interference cancellation scheme in a DS/CDMA system. *IEEE J Sel Areas Commun.* **12** (5), 796-807 (1994).
25. Hui, A., & Letaief, K. Successive interference cancellation for multiuser asynchronous DS/CDMA detectors in multipath fading links. *IEEE Trans Commun.* **46** (3), 384-391 (1998).
26. Whittle, P., Prediction and regulation by linear least-square methods. *J Macroecon.* **7** (1), 126 (1985).
27. Whitesides, G., Ostuni, E., Takayama, S., Jiang, X., & Ingber, D. Soft lithography in biology and biochemistry. *Annu Rev Biomed Eng.* **3** (1), 335-373 (2001).
28. Zhe, J., Jagtiani, A., Dutta, P., Hu, J., & Carletta, J. A micromachined high throughput Coulter counter for bioparticle detection and counting. *J Micromech Microeng.* **17** (2), 304-313 (2007).
29. Song, Y., Yang, J., Pan, X., & Li, D. High-throughput and sensitive particle counting by a novel microfluidic differential resistive pulse sensor with multidetecting channels and a common reference channel. *Electrophoresis.* **36** (4), 495-501 (2015).
30. Watkins, N. et al. Microfluidic CD4+ and CD8+ T lymphocyte counters for point-of-care HIV diagnostics using whole blood. *Sci Transl Med.* **5** (214), 214ra170-214ra170 (2013).
31. Chen, Y. et al. Portable Coulter counter with vertical through-holes for high-throughput applications. *Sensor Actuat B-Chem.*, **213**, 375-381 (2015).
32. Jagtiani, A., Carletta, J., & Zhe, J. An impedimetric approach for accurate particle sizing using a microfluidic Coulter counter. *J Micromech Microeng.* **21** (4), 045036 (2011).
33. Gold, R. Optimal binary sequences for spread spectrum multiplexing (Corresp.). *IEEE Trans. Inform. Theory.* **13** (4), 619-621 (1967).
34. Dinan, E., & Jabbari, B. Spreading codes for direct sequence CDMA and wideband CDMA cellular networks. *IEEE Commun Mag.* **36** (9), 48-54 (1998).

